J|A|C|S
COMMUNICATIONS

Published on Web 01/11/2006

Macroporous Manganese Oxides with Regenerative Mesopores

Eric S. Toberer, Thomas D. Schladt,[#] and Ram Seshadri*

Materials Department and Materials Research Laboratory, University of California, Santa Barbara, California 93106-5121

Received November 22, 2005; E-mail: seshadri@mrl.ucsb.edu

Hierarchically porous materials have attracted recent attention because of the development of new routes to form them and because they are associated with improved efficiencies when used as catalysts or as electrode materials in secondary batteries. Hierarchical porosity enables high surface areas and, hence, high solid−fluid exchange associated with small pores to be combined with the high flow rates associated with large pores. Human lungs are a good example of hierarchical structures that permit large volumes of gas to be exchanged over a large surface area. Recent developments in hierarchically porous inorganic structures have focused on combining templating agents at various length scales. For example, Yang et al.[1] have prepared structures possessing multiple length scales of porosity through a combination of stamping, latex sphere templates, and block copolymer templates. Holland et al.[2] have grown macroporous inverse opals with zeolitic walls, thereby combining microporosity and macroporosity. Anderson et al.[3] have converted diatoms to zeolites while retaining the macropore structures of the diatoms. Blin et al.[4] have used the self-assembly of surfactant micelles to form meso-/macroporous structures of zirconia and titania. Theoretical studies on bimodal pore structures and the anticipated improvements in catalytic efficiency have recently been reviewed.[5]

Our recent efforts on the formation of porous materials using routes that *do not require* pre-structured templates[6] have led us to the discovery that zinc can be leached out of oxides at high temperatures under reducing conditions, yielding a new route to porous oxides and metals.[6d] When this process is applied to macroporous materials, a hierarchically porous product is obtained.[7] Specifically, a dense composite of ZnO and $ZnMn_2O_4$ was rendered macroporous through alkali leaching of the ZnO phase. Mesopores were then induced in the macropore walls through the reduction of the $ZnMn_2O_4$ to rocksalt $Zn_{0.33}Mn_{0.67}O$ with a corresponding volume contraction. The mesoporosity was further increased through the reduction and evaporation of zinc from the rocksalt lattice. The resulting structure possessed a continuous network of 1 μm pores, the walls of which were made up of porous crystals of MnO with 50 nm pores.[7]

Here we describe a unique and simple route to the formation of hierarchically porous MnO by a process of reduction of sintered pellets of Mn_3O_4, with pore formation being induced by volume loss. What is particularly exciting is that this mesopore formation is *cyclable*; oxidizing the final MnO material results in closing of the mesopores without the macropore morphology being altered. Redox cycling thus enables the formation of fresh mesopores in macroporous MnO. Such regenerative pore formation is unprecedented and exciting; a possible application is in catalysis, where deactivation often takes place due to loss of surface area. Processes such as the one presented here can perhaps be used to recreate pores and hence reactivate catalysts. The present work is reminiscent of the concept of "intelligent catalysts" advanced in the field of noble-metal-substituted perovskites, where activity is regained in reducing conditions.[8] We also note here the extensive work on porous manganese oxides by Suib and co-workers.[9]

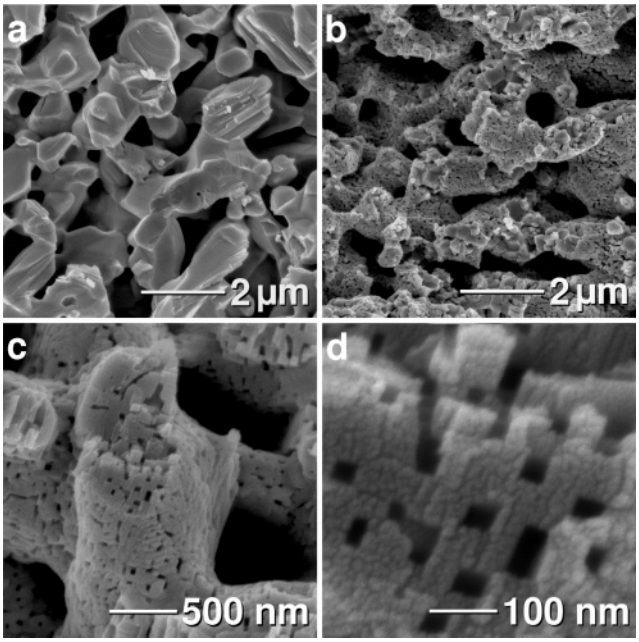

Figure 1. (a) Scanning electron micrograph (SEM) of a Mn_3O_4 pellet formed under conditions that produce porosity. (b) Reduction of the Mn_3O_4 monolith to MnO retains the macroporosity and induces mesopores in the macropore walls, seen clearly at higher magnification in (c). (d) On close inspection, the mesopores are found to be 50 nm on edge, square in shape, and self-affine.

A macroporous monolith of Mn_3O_4 was formed by pelletizing (10 mm diameter × 5 mm thick) and sintering commercial Mn_3O_4 (Aldrich) powder in air at 1125 K for 24 h. The interior fracture surface of the resulting monolith is shown in the scanning electron micrograph (SEM) in Figure 1a. The pore structure and distribution seen in this micrograph are typical of a ceramic body that has been treated under conditions that lead to particle necking but not substantial densification. Despite the porosity, the particles in this monolith are well-connected, and pellets so formed are quite robust. The Mn_3O_4 pore walls were reduced to MnO through heating in an atmosphere of flowing 5% H_2/N_2 at 725 K for 5 h. Figure 1b shows that the macropore network is unaffected by this leaching process, but the macropore walls now display significant mesoporosity (Figure 1c). Scanning electron microscopy of the interior fracture surface reveals a cross-section of one of the grains with 50 nm pores penetrating through it.

As we previously found in MnO formed from reduction and vapor-phase leaching of $ZnMn_2O_4$,[7] the mesopores in the materials obtained here have an approximately rectangular cross-section and

[#] Visiting from the Institut fur Anorganische Chemie, Johannes Gutenberg-Universitat, Mainz, D55099 Germany.

10.1021/ja0579412 CCC: $33.50

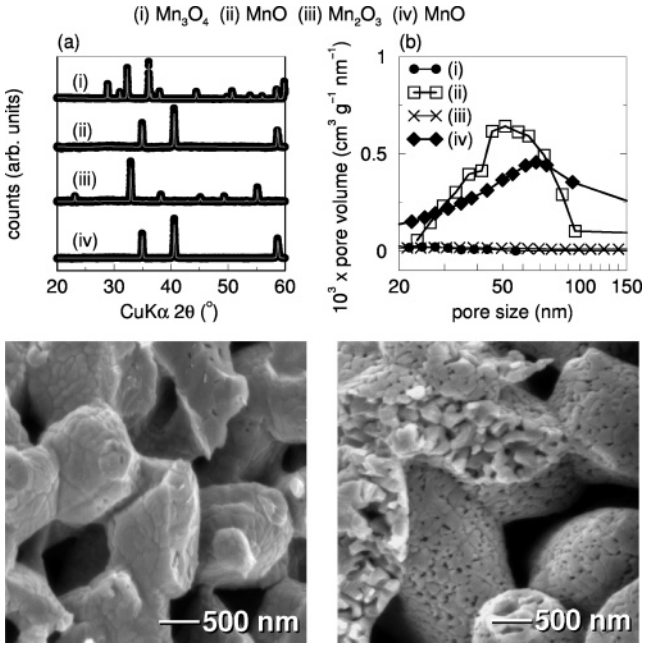

Figure 2. (a) Powder XRD data (points) and Rietveld fits (gray lines) to (i) Mn_3O_4, (ii) MnO obtained by reducing Mn_3O_4, (iii) Mn_2O_3 obtained by oxidizing MnO, and (iv) MnO formed by subsequent reduction. (b) BJH pore size distributions for the materials whose XRD patterns are displayed in panel (a). While the oxidized materials, (i) and (iii), show no mesoporosity, the reduced MnO materials, (ii) and (iv), display mesopores in the 50 nm size range. The SEM image on the left indicates that the Mn_2O_3 material (iii) has lost its mesoporosity, but this mesoporosity is regained upon reduction to MnO (iv), as seen from the image on the right.

are self-affine and aligned with other mesopores, strongly suggesting that pores and walls in Figure 1d are crystallographically related. Through the minimization of surface energy, the cubic rocksalt structure of MnO induces the formation of pores with all walls indexable as {100}, right-angled, and running along three Cartesian directions within each MnO crystallite.

We have monitored phase evolution during the oxidation and reduction process with powder X-ray diffraction and analyzed the data with Rietveld profile refinement using the XND code.[10] Diffraction traces and Rietveld fits to single phases are shown in Figure 2a for (i) the original Mn_3O_4, (ii) MnO formed upon reduction, (iii) Mn_2O_3 formed by reheating in air, and (iv) MnO formed by reducing Mn_2O_3. In all cases, no secondary phase was observed, and the unit cell volumes agreed well with literature values for these structures.

It is clear from the powder XRD traces that, as expected, the phases can be switched back and forth. We have used nitrogen sorption measurements in conjunction with the Barett−Joyner−Halenda[11] analysis of pore size distributions to verify that the process of mesopore formation is regenerative as well, with mesopores in the 50 nm size range forming upon reduction, closing over upon reoxidation, and forming again upon reduction. Figure 2b shows the BJH pore size distributions of the different Mn_3O_4, MnO, and Mn_2O_3 materials whose XRD patterns are displayed in Figure 2a. Mesopore regeneration is clear from these experiments as well as from the SEM images of Mn_2O_3 and MnO displayed in the panels of Figure 2. In agreement with SEM observations, the original material exhibits only pores in the 1 μm regime, while the reduced material has a pore distribution centered about 50 nm. The first reduction increased the surface area from 1 to 6 m^2/g, and the pore volume matches well with the expected volume change associated with the Mn_3O_4 to MnO conversion (expected, 0.038 cm^3/g; measured, 0.037 cm^3/g). Cycling between macroporous Mn_2O_3 and hierarchically porous MnO causes the surface area and pore volume to alternate as expected, although increased dispersion in the pore size distribution is observed during cycling. Higher temperatures in the oxidation step are required to produce Mn_3O_4, and we avoid this as harsher conditions could lead to sintering of the *macropores*.

In conclusion, we have demonstrated that a simple oxide in a high oxidation state can be reduced, with the concurrent loss of volume being accommodated through the formation of mesopores. It helps to think of porous materials as being two phase: solid and void. Complete "phase separation" as would occur for oil and water should yield a dense solid. Instead, what is observed here is that the phase separation results in a perforated solid, in much the same way that block copolymers form complex interpenetrating architectures.[12] While the two blocks in a block copolymer are covalently tethered, in the porous oxides presented here, the "tethering", which prevents complete phase separation, is the high barrier for diffusion of cations in oxides.

Additionally, we have demonstrated a process where the mesopore formation is regenerative in the sense that mesoporosity is lost and regained through a process of oxidation and reduction. We anticipate extensions of the route to a number of different ceramic oxide materials of the transition elements.

Acknowledgment. We gratefully acknowledge support from the National Science Foundation through an IGERT award for E.S.T. (DGE99-87618), through a grant from Chemical Bonding Center (CHE04-34567), and for the use of MRSEC facilities (DMR05-20415).

References

(1) Yang, P.; Deng, T.; Zhao, D.; Feng, P.; Pine, D.; Chmelka, B. F.; Whitesides, G. M.; Stucky, G. D. *Science* **1998**, *282*, 2244−2246.
(2) Holland, B. T.; Abrams, L.; Stein, A. *J. Am. Chem. Soc.* **1999**, *121*, 4308−4309.
(3) Anderson, M. W.; Holmes, S. M.; Hanif, N.; Cundy, C. S. *Angew. Chem., Int. Ed.* **2000**, *39*, 2707−2710.
(4) Blin, J.-L.; Léonard, A.; Yuan, Z.-Y.; Gigot, L.; Vantomme, A.; Cheetham, A. K.; Su, B.-L. *Angew. Chem., Int. Ed.* **2003**, *42*, 2872−2875.
(5) (a) Dogu, T. *Ind. Eng. Chem. Res.* **1998**, *37*, 2158−2171. (b) Kiel, F. J. *Catal. Today* **1999**, *53*, 245−258.
(6) (a) Rajamathi, M.; Thimmaiah, S.; Morgan, P.; Seshadri, R. *J. Mater. Chem.* **2001**, *11*, 2489−2492. (b) Panda, M.; Rajamathi, M.; Seshadri, R. *Chem. Mater.* **2002**, *14*, 4762−4767. (c) Toberer, E. S.; Weaver, J. W.; Ramesha, K.; Seshadri, R. *Chem. Mater.* **2004**, *16*, 2194−2200. (d) Toberer, E. S.; Joshi, A.; Seshadri, R. *Chem. Mater.* **2005**, *17*, 2142−2147.
(7) Toberer, E. S.; Seshadri, R. *Adv. Mater.* **2005**, *17*, 2244−2246.
(8) Nishihata, Y.; Mizuki, J.; Akao, T.; Tanaka, H.; Uenishi, M.; Kimura, M.; Okamoto, T.; Hamada, N. *Nature* **2002**, *418*, 164−167.
(9) (a) Shen, Y. F.; Zerger, R. P.; DeGuzman, R. N.; Suib, S. L.; McCurdy, L.; Potter, D. I.; O'Young, C. L. *Science* **1993**, *260*, 511−515. (b) Tian, Z.-R.; Tong, W.; Wang, J.-Y.; Duan, N.-G.; Krishnan, V. V.; Suib, S. L. *Science* **1997**, *276*, 926−930.
(10) Berar, J.-F.; Bérar, J.-F.; Garnier, P. *NIST Special Publication* **1992**, *846*, 212 (freely available from the CCP14 website at http://www.ccp14.ac.uk).
(11) Barrett, E. P.; Joyner, L. G.; Halenda, P. H. *J. Am. Chem. Soc.* **1951**, *73*, 373−380.
(12) Bates, F. S.; Fredrickson, G. *Phys. Today* **1999**, *52*, 32−38.

JA0579412